Volume 1 | Number 1 | Jan 2013 | Pages 1–100

Nanoscale

www.rsc.org/nanoscale

ROYAL SOCIETY OF CHEMISTRY

ROYAL SOCIETY OF CHEMISTRY

www.rsc.org/nanoscale

Nanoscale

COMMUNICATION

Scribable Multi-walled Carbon Nanotube-Silicon Nanocomposite: A Viable Lithium-Ion Battery System

Rigved Epur[a], Madhumati Ramanathan[b], Moni K. Datta[b], Dae Ho Hong[b], Prashanth H. Jampani[b], Bharat Gattu[c] and Prashant N. Kumta[a,b,c,d,†]

A novel electrode fabrication technique involving a manual scribing action of vertically aligned silicon coated multiwall carbon nanotubes (VASCNTs) on a copper foil have been developed as a viable approach to Li-ion battery electrodes. The scribed electrodes were prepared without the use of any conductive additives and binders; and were directly assembled in a coin cell. These 'binder-less' scribed Si-CNT electrodes exhibited a very high discharge capacity in excess of 3000 mAh/g and a low first cycle irreversible loss (FIR) (19%). Additionally the electrodes also showed good cyclability with capacity retention of 76% at the end of 50 cycles corresponding to a fade rate of 0.48% loss per cycle.

Introduction

Lithium-ion batteries (LIBs) are currently the established and preferred choice of energy storage devices for myriad portable devices such as cell phones, laptops, power tools as well as automotive systems in the form of electric vehicles (EVs) and plug-in hybrid electric vehicles (PHEVs) due to their compact design and high energy density[1]. Currently, the Li-ion battery chemistry used in most practical applications exhibiting energy densities in the range of 100-265 Wh/kg, typically employs graphite as the anode in combination with layered lithium transition metal oxides such as $LiCoO_2$, spinel compounds such as $LiMn_2O_4$ and its high voltage derivatives, as well as the olivine structures involving $LiFePO_4$, as the cathode. However, due to the advancement in power electronics and demand for longer driving range in electric vehicles, batteries possessing much higher energy, power density and cycle life are critically needed. Recently, silicon has garnered enormous interest as an alternative anode to graphite due to its ability to alloy with lithium at electrode potentials similar to that of graphite, forming a highly lithiated phase, $Li_{22}Si_5$, having a theoretical capacity of 4200 mAh/g, which is ten-fold greater than that of graphite (theoretical capacity: 372 mAh/g). However, the formation of this lithiated phase is associated with a colossal volume expansion (>300%) leading to pulverization of the active material contributing to a corresponding large capacity fade[2]. The mechanical failure of silicon has been addressed by implementing approaches that involve controlling the structure, morphology and particle size; so that the capacity retention and cycle life can be significantly improved. These methods typically involve the use of active-inactive matrices[3-6], nanostructured and amorphous form of silicon such as silicon nanoparticles[7], nanowires[8,9], nanotubes[10,11] and other nanoscale architectures[12-16].

In all the hitherto reported approaches, the conventional slurry casting approaches are used for fabricating the electrodes. This traditional method of preparing electrodes for a Li-ion battery involves the mixing of active material with a conductive additive and binder which is then casted onto a metallic foil. After drying these foils thoroughly, the dry laminate is cut out into required shapes and is later assembled along with separator, electrolyte and other packaging components to form a battery pack. Among the various components, the conductive additives and binders on the laminate primarily form the electrochemically inactive components and which add and contribute to the dead weight and volume of the electrode, thereby decreasing the overall specific capacity of the electrode. To overcome this, several 'binder-less' approaches were explored for silicon based anodes, wherein, the active material has been grown directly onto the copper foil using various techniques comprising electrodeposition[17,18], RF sputtering[19,20] and chemical vapour deposition[11-13,21]. For instance, in one of our earlier works, heterostructures of vertically aligned multiwall carbon nanotubes (VACNTs) decorated with silicon droplets were directly grown on Inconel 600 foil to form vertically aligned silicon and carbon nanotube (VASCNTs) composites which were then directly assembled into a coin cell without the use of binders or conductive additives[13]. In this case, the carbon nanotubes served as a mechanically robust scaffold to accommodate the large stresses generated in the silicon droplets during the lithiation and de-lithiation processes, and additionally provided good electronic conductivity to facilitate charge-transfer. All the binder-less techniques that have been explored so far required the current collector to be used as the substrate during the silicon growth process. This in turn imposes several limitations such as: inability of the current collector to withstand the reaction conditions such as high corrosive electroplating baths; possible side reactions such as iron silicide formation during CVD[8] and low yield limited by the size of the reactor.

In this work, we demonstrate a novel technique for fabricating a simple 'binder-less' scribable electrode comprising silicon coated multiwall carbon nanotubes (VASCNTs). The VASCNTs were developed by a two-step chemical vapor deposition approach[12-14] and is made into a pellet which was used to manually scribe on a copper foil to achieve the active material coating. This method does not involve the use of any binders or conductive additives, offering the capability to coat large areas of the current collector and additionally, significantly reducing the processing time.

Results and Discussion

Figure-1 shows the various steps involved in the fabrication of the scribed electrodes comprising generation of the multiwall carbon nanotubes followed by coating them with silicon at different stages. Long vertically aligned multiwall carbon nanotubes (VACNTs) were first grown on a quartz slide using a simple liquid injection approach similar to our earlier published work where ferrocene and m-xylene were used as the catalyst and carbon source for the growth of the carbon nanotubes, respectively[12-14]. Amorphous Si was then deposited following the protocol described in the methods section. The obtained VASCNT heterostructures were compacted using a uniaxial press into a pellet (diameter=13 mm, height= ~2 mm) which was then used to manually scribe the VASCNT on a copper foil employing a conventional writing action. A uniform dark coverage of the Si-CNT composite film was obtained within few strokes of the scribing action (See video S1 in Supplementary Data). A mechanical roller was then used to further press the coated electrodes to enhance the adhesion of the VASCNT nanocomposite on the Cu foil to form the Si-CNT nanocomposite electrode.
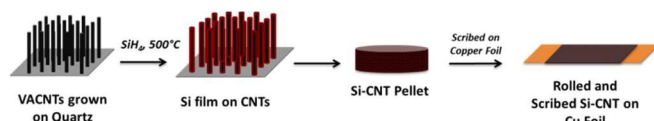

Fig.1: Schematic showing the fabrication of scribable Si-CNT electrode on copper foil.

Figure-2 shows the SEM images of the Si-CNT hetereostructures at various stages of the synthesis and electrode preparation. Figure-2a shows the vertically aligned dense carbon nanotubes obtained on quartz with lengths in the 200 μm - 300 μm range and diameters in the range of 25-35 nm[12]. Following silane decomposition, the silicon is coated as a uniform thin layer on the CNTs as displayed in the SEM image in Figure-2b. Figures - 2c & 2d show the SEM images of the Si-CNTs present in the pressed pellet and on the copper foil obtained after the scribing action, respectively. Figure-2e shows the high resolution image of the Si-CNTs which indicates the uniform coating of silicon in the range of 25-30 nm around the CNTs. Some amount of shortening of the overall length of the heterostructures can be noticed which may be due to the application of large load during the compaction process leading to fracture of the CNTs. However, it should be noted that the silicon coating on the VACNTs remained intact even after compaction by cold-pressing followed by the scribing action on the copper foil. This is possibly due to the strong Van der Waals forces that hold the vertically aligned carbon nanotubes together similar to what is seen in the CNT yarns made by the dry spinning methods[22]. In this case, the scribing action of the Si-CNT pressed pellet on the copper foil enables the individual silicon coated carbon nanotubes to glide over each other adhering physically to the surface of the copper foil similar to the published report[23].
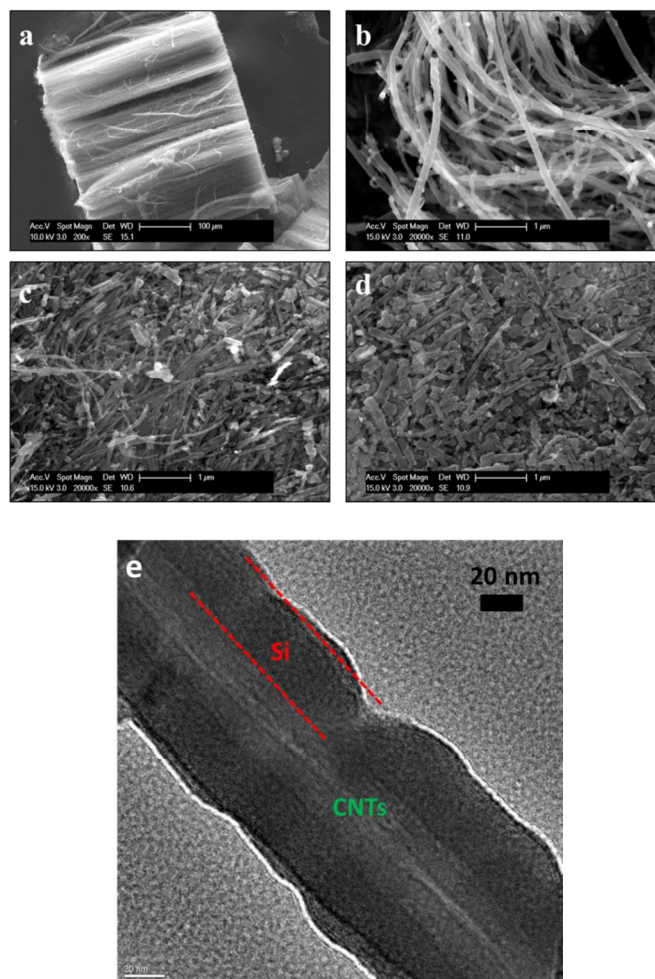

Fig.2: SEM images of (a) vertically aligned carbon nanotubes grown on quartz (VACNTs), (b) VACNTs coated with silicon (VASCNT), (c) Si-CNTs after being pelletized by cold pressing, d) Si-CNTs after being scribed and rolled on Cu and (e) HRTEM image of the silicon coated CNTs.

X-ray diffraction patterns obtained on the SiCNT composite displayed in Figure-3a indicate sharp peak corresponding to the (002) planes of the multiwall carbon nanotubes due to the hexagonal arrangement of sp^2 hybridized carbon atoms. Peaks corresponding to crystalline silicon are also observed along with a dominant amorphous phase indicated by the presence of two broad humps close to the 2 theta (2θ) angle of 25° and 55°. The location of the first and short range order peaks or the broad humps of this amorphous phase is consistent with our previous reports wherein this phase was attributed to amorphous silicon[12]. Raman spectroscopy was also performed to analyse the amorphous phase and detect the Raman vibrational states of Si. Figure-3b shows a broad peak centred at approximately 475 cm^{-1}. Studies show that for crystalline silicon, a sharp peak at 520 cm^{-1} is usually observed in the Raman spectra which corresponds to the transverse optical (TO) phonon vibration and as the crystallite size decreases, this peak becomes broader and shifts to lower values [24-26]. Absence of the sharp peak at 520 cm^{-1} suggests that the silicon present is completely amorphous. Another small peak observed at 300 cm^{-1} is consistent with the longitudinal acoustic phonon mode for amorphous silicon. Hence from the x-ray and Raman studies, it can be concluded that the

COMMUNICATION

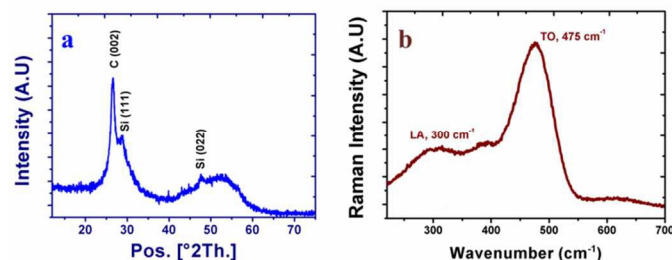silicon deposited by CVD is predominantly amorphous, with a very small amount of crystalline silicon.

Fig.3: (a) XRD pattern & (b) Raman spectra of the Si-CNT nanocomposite obtained after the CVD process.

As mentioned earlier, in addition to the electrochemically active material that is present in a typical lithium-ion battery electrode, electrochemically inactive components such as conductive additive and binder that add to the undesirable additional weight and volume of the electrode are also present in the cast electrode slurry. Conductive additives are added to provide the inter-particle electronic conductivity while the binder aids in holding all the components (active and inactive) to the current collector. The scribed electrode containing the Si-CNTs nanocomposite contains the electronically conducting MWCNTs at the inner core while also displaying a strong adherence to the current collector, thereby eliminating the need to use any conductive additives and additional binders. These scribed electrodes are thus directly assembled in a coin cell (CR 2025) configuration for studying their electrochemical properties. Figure-4a shows the voltage vs. capacity plot of the scribed Si-CNT nanocomposite electrode corresponding to the 1st, 2nd and 50th cycles obtained at a current density of 300 mA/g when cycled between the voltage range 0.01V to 1.0 V vs. Li^+/Li in a half cell configuration. It can be seen clearly that lithiation during the first cycle resulted in a very high discharge capacity of 3112 mAh/g close to the expected theoretical capacity ~3780 mAh/g determined from the silicon content discussed below. This close match despite the moderately large current rate is reflective of the promise offered by the approach. During the subsequent de-lithiation, a charge capacity of 2523 mAh/g was obtained resulting in a first cycle irreversible (FIR) loss of only 19% which is comparable to the commercially available graphite based anodes and similar to our earlier report[14]. The large capacity of 3112 mAh/g obtained assuming all of the Si deposited on the 200-300 μm aligned CNT of diameter 25-35 nm that is scribed onto the Cu foil is electrochemically active; provides an electrode thickness of ~400 μm for an approximate Si film thickness of ~0.2-0.4 μm, further suggesting the efficacy of the approach. A very high first discharge capacity as mentioned above suggests that the Si-CNT nanocomposite is mainly composed of silicon, owing to the low density of the underlying MWCNTs. Thermogravimetric (TGA) analysis performed on the Si-CNT composite indicated the amount of silicon to be close to 90 wt% in the Si-CNT composite (Figure-S2), which corresponds to a theoretical capacity of 3780 mAh/g. According to our previous reports[12], the CNTs below the silicon coating can be considered to not contribute to any significant capacity. Hence accordingly, in the current work, the CNT was not included in calculating the theoretical capacity of the electrode. The different lithiation and de-lithiation reactions that occur during the charge-discharge processes are usually observed as voltage plateaus in the voltage vs. capacity plots. However, the differential capacity plots provide a better representation of the reaction as indicated by the peaks in contrast to plateaus. Further, as shown in Figure-4b, during the 1st cycle lithiation, a large peak at 0.2 V is observed followed by a bell shaped curve at 0.09 V. The peak at 0.2 V corresponds to the voltage plateau in Figure-4a which indicates the presence of a two phase region governed by the Gibbs phase rule. These phases correspond to the unlithiated amorphous silicon (a-Si) and partially lithiated silicon phases (Li_xSi) that co-exist until the voltage reaches 0.1 V wherein complete lithiation of the parent amorphous silicon phase occurs to yield the amorphous Li_xSi phase takes place [12, 13, 20, 27]. Below 0.1 V, further lithiation of Li_xSi phase continues to occur along with lithiation of any crystalline silicon present and is represented by the bell curve centred at 0.09 V. During the de-lithiation step, two major peaks are observed at 0.28 V and 0.43 V which represent the de-lithiation reactions between the lithiated amorphous silicon phases[20, 27]. In the 2nd cycle however, the first lithiation reaction now appears to occur at a slightly higher voltage at around 0.24 V and is consistent with our earlier published reports using amorphous silicon[6, 12, 20]. The differential capacity curves for the de-lithiation reactions for 1st and 2nd cycles overlap well indicating the absence of any other additional reactions.

The cycling stability plot or the charge-discharge plot for several cycles shown in Figure-4c indicates the reversibility of the Si-CNT electrode. After the first cycle irreversible loss (FIR), the SiCNT electrode exhibits good cyclability and stability for 50 cycles with very little capacity fade compared to commercial silicon electrodes. At the end of 50 cycles, capacities close to 2000 mAh/g were obtained when cycled at the current of 300 mA/g which represents a capacity retention of ~76% (calculated with respect to capacity obtained from the 2nd cycle) and a fade rate of 0.48% loss per cycle. The Coulombic efficiency calculated at the end of the 2nd cycle was 96% which subsequently improved upon repeated cycling reaching a value of 98.5 % at the end of 50 cycles. The low Coulombic efficiency in the early stages of cycling may be due to the formation of a stable solid electrolyte interphase (SEI) layer or due to the irreversible intercalation of Li^+ ions into the defect sites of the multiwall carbon nanotubes as is known.

Rate capability is an important characteristic for the battery which relates its performance or the amount of charge stored at various current densities (load). Figure-4d shows the rate capability plot performed at 100, 250, 500, 1000 and 2000 mA/g. No significant reduction in capacity can be observed as the current densities were steadily increased from 100 mA/g to 2000 mA/g. Capacities greater than 1500 mAh/g can be obtained even for very high current densities of 2000 mA/g which is nearly five-fold greater than the capacity obtained using commercial graphite anodes.
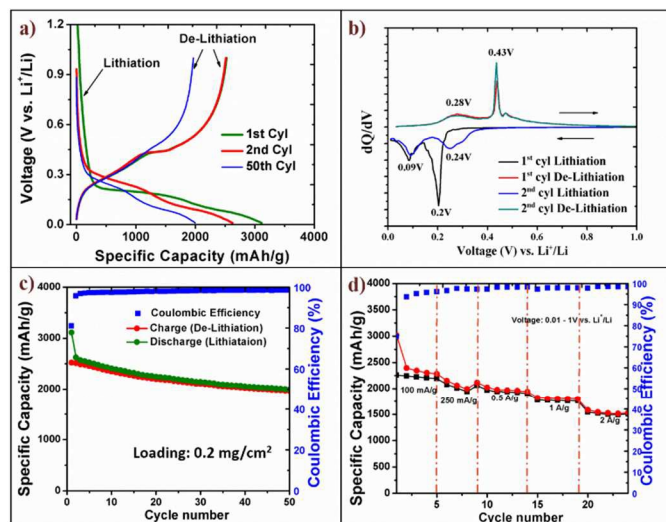
Fig.4: Electrochemical characteristics of the scribed Si-CNT pellet on copper foil: (a) voltage vs. capacity plot (b) differential capacity plot (c) charge-discharge cycles conducted at 300 mA/g between 0.01 to 1 V vs. Li^{+}/Li (d) rate capability plot obtained at 100, 250, 500, 1000 and 2000 mA/g between 0.01 to 1 V vs. Li^{+}/Li.
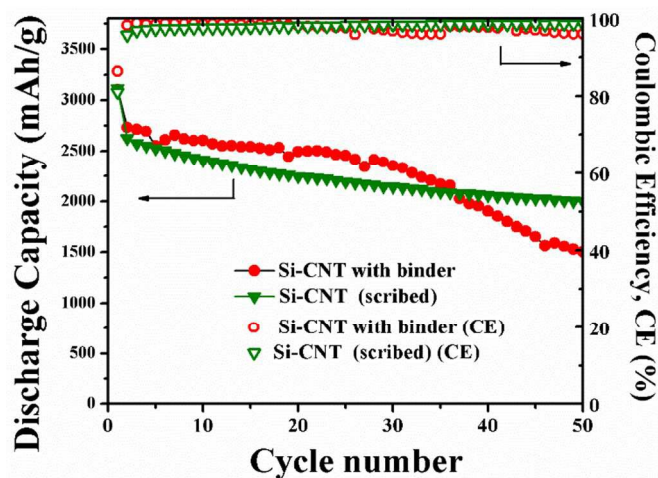

Fig.5: Discharge capacities of the scribed Si-CNT pellet (green triangle) and Si-CNTs prepared by slurry cast method (red circle). All electrode were at 300 mA/g between 0.01 to 1 V vs. Li^{+}/Li.

A comparative electrochemical study was also conducted on Si-CNTs prepared by conventional slurry casting technique involving the use of conductive additive (Super-P) and binder (sodium carboxymethyl cellulose, CMC). Figure-5 shows the discharge (lithiation) capacity plots of Si-CNT electrodes prepared by the slurry casting and scribed techniques. The specific discharge capacity of the cast electrodes was calculated based only on the active material content (Si and CNTs). It is observed that during the initial stages of cycling, the electrochemical characteristics of the slurry cast electrodes are comparable to that of the scribed electrodes such as high first discharge capacity (3102 mAh/g) and low first cycle irreversible loss (14%). However, the slurry cast electrodes show good cyclability only up to 30 cycles, showing a capacity of 2350 mAh/g (for 30th cycle), after which a rapid capacity fade can be observed. At the end of the 50th cycle, the slurry cast electrodes show a capacity of only 1500 mAh/g with a capacity retention of 55% (fade rate: 0.9% loss/cycle for 50 cycles). In the case of the scribed electrodes, the capacity fade is relatively more gradual and uniform, devoid of any region containing rapid capacity loss. The capacity fade for the slurry cast electrodes could arise from various factors such as SEI layer formation, loss of particle contact (electrical contact between the Si and CNT; and electrical contact between Si-CNT and current collector via failure of the binder/Super-P). The exact mechanism contributing to the rapid capacity loss at 30 cycles of these CVD derived Si/CNT slurry cast electrodes is currently not known. Further studies such as in-situ SEM or in-situ TEM studies are warranted to understand these failure mechanisms and could eventually provide an understanding to the different fade rates for the scribed and slurry cast electrodes.

Furthermore, in order to demonstrate the structural integrity of the electrode with repeated cycling, post cycling analysis of the electrodes was performed using scanning and transmission electron microscopy techniques. Figure-6a shows the SEM image of the scribed CNT/Si heterostructures after 50 cycles (at 300 mA/g between 0.01 to 1V vs. Li^{+}/Li). It is observed that the morphology of the electrode after 50 cycles is very comparable to the original scribed CNT/Si electrode before cycling (Figure-2d). The short CNT segments are still observed with a more rugged surface, which can be attributed to the well-known solid electrolyte interphase (SEI) formation. These SEI coated CNT/Si segments are still well connected electrically to each other and is mainly responsible for the good cyclability observed. In our previous studies on the CVD generated CNT/Si heterostructures, we have observed and validated using electron energy loss spectroscopy (EELS), that a thin amorphous carbon layer is formed at the interface between the CNT and Si surfaces.[14] This amorphous carbon layer acts as a strongly bonded interface that serves to tether the Si droplets to the CNT surface. This results in improved electrochemical stability by maintaining a good electrical contact between Si and CNT even during the repeated lithium alloying and de-alloying processes. In this approach, a similar phenomenon is expected to occur wherein a strong interface between CNT and Si due to the interfacial amorphous carbon layer can be accounted for the good electrochemical performance and cyclability in addition to the good adhesion of the active material to the copper current collector due to the large mechanical force applied. Figure-6b shows the high resolution TEM image of the Si-CNT interface after 50 cycles. The CNT structure along with Si coating and the Si-CNT interface is well preserved showing the overall structural integrity even after 50 cycles owing to the good interfacial bonding due to the amorphous carbon layer likely formed between the CNT and Si as reported in our earlier publication[14].
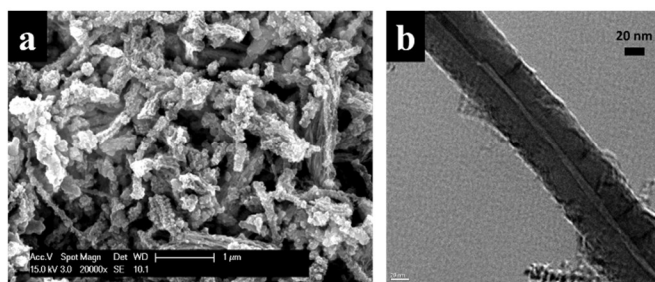
Fig.6: (a) SEM images and (b) TEM images of the scribed Si-CNTs after 50 cycles of charge and discharge (at 300 mA/g between 0.01 to 1 V vs. Li$^+$/Li).

To examine the charge transfer resistance characteristics of the scribed electrodes, electrochemical impedance analysis was conducted and Figure-7 shows the Nyquist plots obtained from the impedance tests performed on the cells following de-lithiation reactions at the end of 1st and 50 cycles. The plot in general, is characterized by a semi-circular region at the higher frequencies and this is associated with the good electronic conductivity of the electrodes arising from the facile electron transfer processes occurring within the CNTs during the lithiation and de-lithiation reactions occurring at the interface of the Si-CNTs and the electrolyte. The linear region at the lower frequencies is attributed to diffusion limited processes. The inset in Figure-7 represents the equivalent circuit that was modeled to best describe the electrode interface of the battery that was examined. As shown in the circuit, the physical structure of the electrode interface may be represented using a combination of a resistor and constant phase element (CPE) corresponding to the semi-circle at higher frequencies; and a Warburg element at lower frequencies, respectively.
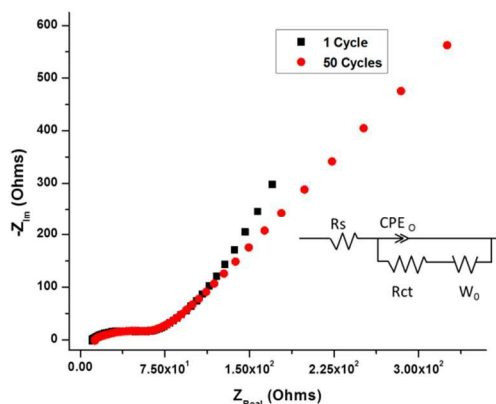

Fig.7: Impedance spectra of the Si-CNT nanocomposite scribed electrodes after the de-lithiation step at the end of 1st and 50th cycles.

From Table-1, it can be observed that the charge transfer resistance (R_{ct}) generated from modeling the equivalent circuit, does not show a significant change in the electrode impedance following 50 cycles of charge and discharge, thus indicating the possible absence of pulverization of the scribed CNT-Si films that may generate new electrochemically active surfaces or lead to compositional and chemical changes. The scribed Si-CNT nanocomposite electrodes generated by the simple scribing action thus exhibit high capacity, good electrochemical stability. The

coatings generated by the scribing action are relatively thick and are devoid of any conductive additives and binders thus adding to the efficacy and overall efficiency of the electrode fabrication process in general.

Table-1: Charge transfer resistance (Rct) values obtained after 1st and 50th charge/discharge cycles showing minimal increase in the overall resistance

	After 1st cycle	After 50 cycles
Charge transfer resistance (R_{ct}), ohms	37.23	41.29

Similar electrode configuration can be designed for the cathodes in the future wherein, thin film coatings of compounds such as $LiCoO_2$, LMn_2O_4 and $LiFePO_4$ could be easily grown on the CNTs which could eventually be scribed onto aluminium foils, leading to the development of an 'all-scribable' Li-ion battery, potentially a viable approach to high energy density battery configurations. These studies are on-going and will be reported in the near future.

Materials and Methods

VASCNT nanocomposite preparation

Multiwall carbon nanotubes (MWCNTs) were first grown in a horizontal quartz tube furnace using a floating catalyst method[12-14]. Ferrocene was dissolved at 0.1 g/ml concentration in m-xylene, wherein the iron nanoparticles derived from ferrocene aided the growth of the vertically aligned carbon nanotubes while m-xylene served as the carbon source. The catalyst-carbon source solution was fed continuously at a rate of 0.11 ml/min into a stainless steel gas bubbler maintained at 200°C before entering the CVD reactor. Argon and hydrogen were used as the carrier gases flowing at 85 sccm and 15 sccm, respectively. A quartz slide was used to grow the CNTs at 770°C for a 90 minute deposition time.

Amorphous silicon (*a*-Si) was deposited by thermal cracking of silane gas (SiH_4) in a low pressure chemical vapor deposition reactor (LPCVD). The MWCNTs grown on the quartz substrate were placed in the center of the quartz tube (outer diameter=42 mm) and purged thoroughly with argon gas and vacuumed to remove any residual oxygen present in the tube. For silicon deposition, 3.33% silane (diluted in argon gas) was decomposed at 500°C for a total deposition time of 20 minutes. After the deposition, the reactor was cooled down and opened when the temperature was below 100°C to avoid any silicon oxidation. The obtained *a*-Si coated MWCNT (VASCNT) composite was collected, and used for pellet preparation and other characterization studies.

VASCNT pellet preparation

The scribable pellets comprising Si-CNTs were prepared as follows. 200 mg of the VASCNTs generated as described above were pressed using a uniaxial cold press (Carver Inc, IN) under a load of 5 Tons for 60 seconds into a pellet (diameter=13 mm, height= ~2 mm). The cold pressed pellets were then used as a pencil

lead to scribe on a copper foil (18 µm thick, Insulectro) (See video S1 in the Supplementary Data). For better adhesion, the SiCNTs scribed on the copper foil were pressed using a cylindrical roller (MTI Corp, CA). The loading achieved with the scribed electrodes was ~0.2 mg/cm^2. Also, in a parallel study, slurries of Si-CNTs were prepared using sodium carboxymethyl cellulose binder (CMC, MTI Corp, CA) and Super-P (MTI Corp, CA) (Si-CNT:CMC:Super-P=50:40:10). The Si-CNT slurry was casted onto the copper foil using a doctor blade technique and dried overnight at 100°C in vacuum. Electrodes of 9 mm diameter (scribed and slurry cast) were cut using a precision disc cutter (MTI Corp, CA) which essentially served as the working electrode for further materials and electrochemical characterization.

Materials and electrochemical characterization

X-Ray diffraction analysis was performed on the SiCNT pellet using a Philips XPERT PRO system (Cu Kα, λ = 0.15406 nm radiation) to analyze the phases present. At the same time, structural characteristics of the synthesized nanocomposite was determined by Raman spectroscopy using a Renishaw in Via Raman microscope equipped with a 633 nm red diode laser. Scanning electron microscopy (SEM) was employed to study the composite morphology using a Philips XL30 operating at 10-20kV. High resolution transmission electron microscopy (HRTEM) studies were done using JEOL JEM-2100F microscope.

Electrochemical measurements were conducted on the scribed electrodes. The electrodes were generated by directly assembling the scribed SiCNT electrodes prepared on Cu foils in CR 2025 coin cells in an oxygen and moisture free glove box (Innovative Technologies Inc). Pure lithium foil was used as the counter electrode in a half cell configuration and a Celgard 2250 polyethylene was used as the separator (MTI Corp, CA). The electrolyte was composed of 1M LiPF$_6$ salt dissolved in the solvent of composition: ethylene carbonate (EC)/diethyl carbonate (DEC)/fluoroethylene carbonate (FEC)=45/45/10 (BASF, NJ). Following the assembling step, the cells were aged for a minimum of 6 hours before performing the electrochemical tests in order to ensure good wettability of the electrolyte with the fabricated electrodes. All the charge-discharge tests were studied using an Arbin Potentiostat (Arbin Instruments, TX) between 0.01V and 1.0 V vs. Li$^+$/Li. A Gamry 4G 300 potentiostat (Gamry Instruments, Warminster, PA) was used for electrochemical impedance characterization. Impedance scans were recorded after the de-lithiation reaction at the end of the 1st and 50th cycles, over a frequency range 0.1 Hz to 300 Hz utilizing an AC stimulus of 10 mV bias at open circuit potential. The cells were aged for 4 hours after the de-lithiation step before performing any impedance analysis.

Conclusions

Herein, we report a simple and facile, novel scribable technique for achieving electrochemically active moderately thick Si-CNT nanocomposite coatings on copper foil. The Si-CNT heterostructures synthesized by the simple 2-step chemical vapor deposition technique were compacted into a pellet using conventional cold pressing technique that were then used to scribe the electrode on a copper foil to form the final electrode devoid of any additives and binders. A very high first discharge capacity of 3112 mAh/g was obtained followed by a low first cycle irreversible loss (19%). The scribed electrodes also exhibited good cyclability with 76% capacity retention at the

end of 50 cycles, corresponding to a fade rate of 0.48% loss per cycle. Impedance studies performed at the beginning and at the end of the charge-discharge tests do not show any significant increase in charge transfer resistance correlating to the good cyclability of the scribed Si-CNT electrodes suggesting the approach to be a viable strategy for high energy density electrodes.

Notes and references

[a]Department of Mechanical Engineering and Materials Science, University of Pittsburgh, Pittsburgh, PA 15261 – USA
[b]Department of Bioengineering, University of Pittsburgh, Pittsburgh, PA 15261 – USA
[c]Department of Chemical and Petroleum Engineering, University of Pittsburgh, Pittsburgh, PA 15261 – USA
[d]Center for Complex Engineered Multifunctional Materials, University of Pittsburgh, Pittsburgh, PA 15261 – USA

†Address correspondence to:
815C Benedum Hall
Department of Bioengineering, Chemical and Petroleum Engineering, Mechanical and Engineering and Materials Science
3700 O'Hara Street,
University of Pittsburgh
Pittsburgh, PA 15261
Email: pkumta@pitt.edu

Electronic Supplementary Information (ESI) available:

1. Video S1: video showing the preparation of the SiCNT pellets and subsequent scribing on copper foils to form the electrodes
2. Figure S2: TGA plot of CNT/Si heterostructures performed in air from 25°C to 1000°C at a heating rate of 10°C/min

1. M. Armand and J. M. Tarascon, *Nature*, 2008, **451**, 652-657.
2. L. Y. Beaulieu, K. W. Eberman, R. L. Turner, L. J. Krause and J. R. Dahn, *Electrochemical and solid-state letters*, 2001, **4**, A137-A140.
3. I. Kim, G. E. Blomgren and P. N. Kumta, *Electrochem. Solid State Lett.*, 2003, **6**, A157-A161.
4. I. Kim, P. N. Kumta and G. E. Blomgren, *Electrochem. Solid State Lett.*, 2000, **3**, 493-496.
5. I. S. Kim, G. E. Blomgren and P. N. Kumta, *Journal of Power Sources*, 2004, **130**, 275-280.

6. W. Wang and P. N. Kumta, *Journal of Power Sources*, 2007, **172**, 650-658.

7. X. H. Liu, L. Zhong, S. Huang, S. X. Mao, T. Zhu and J. Y. Huang, *Acs Nano*, 2012, **6**, 1522-1531.

8. C. K. Chan, H. L. Peng, G. Liu, K. McIlwrath, X. F. Zhang, R. A. Huggins and Y. Cui, *Nat. Nanotechnol.*, 2008, **3**, 31-35.

9. I. Ryu, J. W. Choi, Y. Cui and W. D. Nix, *Journal of the Mechanics and Physics of Solids*, 2011, **59**, 1717-1730.

10. M. H. Park, M. G. Kim, J. Joo, K. Kim, J. Kim, S. Ahn, Y. Cui and J. Cho, *Nano Letters*, 2009, **9**, 3844-3847.

11. H. Wu, G. Chan, J. W. Choi, I. Ryu, Y. Yao, M. T. McDowell, S. W. Lee, A. Jackson, Y. Yang, L. B. Hu and Y. Cui, *Nat. Nanotechnol.*, 2012, **7**, 309-314.

12. R. Epur, M. K. Datta and P. N. Kumta, *Electrochimica Acta*, 2012, **85**, 680-684.

13. W. Wang, R. Epur and P. N. Kumta, *Electrochem. Commun.*, 2011, **13**, 429-432.

14. W. Wang and P. N. Kumta, *ACS Nano*, 2010, **4**, 2233-2241.

15. S. Zhou, X. H. Liu and D. W. Wang, *Nano Letters*, 2010, **10**, 860-863.

16. R. Krishnan, T. M. Lu and N. Koratkar, *Nano Letters*, 2011, **11**, 377-384.

17. R. Epur, M. Ramanathan, F. R. Beck, A. Manivannan and P. N. Kumta, *Materials Science and Engineering: B*, 2012, **177**, 1157-1162.

18. X. Chen, K. Gerasopoulos, J. Guo, A. Brown, C. Wang, R. Ghodssi and J. N. Culver, *Advanced Functional Materials*, 2011, **21**, 380-387.

19. M. K. Datta, J. Maranchi, S. J. Chung, R. Epur, K. Kadakia, P. Jampani and P. N. Kumta, *Electrochimica Acta*, 2011, **56**, 4717-4723.

20. J. P. Maranchi, A. F. Hepp and P. N. Kumta, *Electrochem. Solid State Lett.*, 2003, **6**, A198-A201.

21. T. Song, J. L. Xia, J. H. Lee, D. H. Lee, M. S. Kwon, J. M. Choi, J. Wu, S. K. Doo, H. Chang, W. Il Park, D. S. Zang, H. Kim, Y. G. Huang, K. C. Hwang, J. A. Rogers and U. Paik, *Nano Letters*, 2010, **10**, 1710-1716.

22. A. Ghemes, Y. Minami, J. Muramatsu, M. Okada, H. Mimura and Y. Inoue, *Carbon*, 2012, **50**, 4579-4587.

23. K. A. Mirica, J. G. Weis, J. M. Schnorr, B. Esser and T. M. Swager, *Angewandte Chemie International Edition*, 2012, **51**, 10740-10745.

24. R. L. C. Vink, G. T. Barkema and W. F. van der Weg, *Physical Review B*, 2001, **63**, 115210.

25. J. H. Parker, Jr., D. W. Feldman and M. Ashkin, *Physical Review*, 1967, **155**, 712.

26. C. Smit, R. van Swaaij, H. Donker, A. Petit, W. M. M. Kessels and M. C. M. van de Sanden, *Journal of Applied Physics*, 2003, **94**, 3582-3588.

27. L.-F. Cui, R. Ruffo, C. K. Chan, H. Peng and Y. Cui, *Nano Letters*, 2008, **9**, 491-495.